Exploring the Effect of Base Compliance on Physical Human-Robot Collaboration

Ziqi Wang[1] and Marc G Carmichael[1]

***Abstract*— Mobile physical human-robot collaboration (pHRC) using collaborative robots (cobots) and mobile robots has attracted much research attention. Many researchers have focused on improving the control performance to comply with human intentions. However, a problem that generally exists with mobile pHRC but often gets neglected is the impact of non-rigid components e.g. deformable tyres, suspension systems and uneven terrain on human interaction experience and task performance. To fullfil this current research gap, we carried out an investigation on the above-mentioned problem by altering a cobot's base rigidity level (also referred to as *base compliance level* or *BCL*) during pHRC experiments. We explored how the task performance is affected by base compliance as well as human operator's experience and cobot control parameters. Measurements include the human operator's physical effort, task velocity, and task error. From the experimental results, it is discovered that base compliance has a significant impact on task accuracy as it can easily excite the system if an inadequate control strategy is deployed. Furthermore, through ANOVA, it is discovered that the influence of base compliance can be minimized and system excitation can be avoided by sufficient human operator training and the appropriate selection of cobot's control parameters.**

I. INTRODUCTION

Physical human-robot collaboration (pHRC) entails direct physical contact between the human hand and the collaborative robot's (cobot) end-effector [1], and combines the human's perception and decision making skills with the high consistency, endurance and precision of robots. Using pHRC to assist industrial tasks such as industrial abrasive blasting [2], material sawing and surface polishing [3] and object handling [4] has been developed by researchers.

The shared workspace of the human-robot team is generally limited since the robot is commonly mounted on a rigid base, fixed in the environment. To increase this shared workspace and enable more functionalities, cobots can be mounted to wheeled mobile robots (WMR) to achieve mobile pHRC so that they can work in the unlimited workspace. Nevertheless, a new issue arises. The combined weight of the mobile robot's chassis, the cobot and the tool attached at its end-effector could deform the WMR's wheels and suspension system. As shown in Fig.1, the interactive dynamics will propagate from the end-effector to the base of the cobot through the kinematics chain, and eventually excite a compliant mobile robot through the coupling between the cobot and the WMR. This will result in cobot vibrations and system instability, potentially affecting the human interaction

[1]Ziqi Wang and Marc G. Carmichael are with the Robotics Institute, Faculty of Engineering and Information Technology, University of Technology Sydney, Broadway, Ultimo NSW 2007, Australia.
Email: marc.carmichael@uts.edu.au

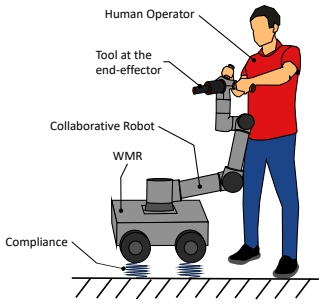

Fig. 1. Illustration of system compliance during pHRC.

experience and reducing task accuracy. Besides the load, the terrain on which the WMR operates could also introduce instability and excite the mobile pHRC system. For example, when WMR drives on soft or uneven terrains, its wheels and suspension springs will be frequently compressed and extended, resulting in wobbling motions. The above-mentioned paradigms that introduce undesired motions to the mobile pHRC framework are referred to as *compliance* in this paper. Even though compliance generally exists for overground mobile pHRC, to the author's knowledge, its impact on the human interaction experience and task performance has never been studied systematically, and base compliance is rarely considered when developing pHRC controls.

This work addresses the research gap in the pHRC discipline by empirically investigating how the base compliance of a cobot affects a pHRC task. A specially made robot base with controllable compliance characteristics is utilized to systematically investigate its effects. In addition, the effects of cobot control parameters and human experience are also included. The main contributions of this paper are the validation of a pHRC challenge through a novel experimental framework; and the identification of significantly influential factors.

The rest of this paper is structured as follows: Section II summarizes related existing works; Section III presents our experimental design and procedure; Section IV presents the experimental results; The limitations of this study and future work are discussed in Section V; Finally, conclusions are drawn in Section VI.

II. RELATED WORK

The problem of controlling the manipulator while suppressing base vibration has been widely researched in the

area of flexible manipulators. Because of lightweight materials and the non-rigid base, the problems of link deflection and base vibration are associated with flexible manipulators. To ensure task precision and the safety of equipment, scholars have proposed many novel solutions [5]–[13].

Fu [5] analyzed the influences of a flexible base, flexible links and flexible joints of a space manipulator to achieve trajectory tracking with vibrations suppression. Trajectory tracking is achieved by a fixed time sliding mode control. The link deflection and base vibration are decomposed separately from the whole-body dynamic model and suppressed by linear quadratic optimal control. Similarly, in [7], [8], the base and flexible arms vibrations are also decomposed from the whole-body dynamics. In the former, an optimal linear quadratic regulator controller is adopted to damp out the system vibrations and an adaptive fuzzy controller is designed to suppress system vibrations in the latter. In [10], the authors considered a flexible manipulator on a rotatable base and proposed an adaptive fault-tolerant boundary control method. The angles of the manipulator and the base are tracked and the deflection and vibration are also eliminated simultaneously; Likewise, [9] also proposed a boundary control law to regulate the flexible manipulator's orientation while suppressing elastic vibration. In [12], a 6-axis force-torque sensor is used at the base of the macro/micro manipulator. From the measured reaction force/torque, feedback control is implemented. Alongside the visual servo control, precise positioning of payloads and base vibration suppression are realized.

Despite the success in suppressing system vibrations in the aforementioned papers, their proposed solutions are not considered for the pHRC application. In these studies, vibration suppression is achieved for the trajectory tracking problem and humans are not included in the control loop. [6] and [13] addressed the problem from the path planning stage. In the former, a virtual control force is used to generate the trajectory that can stabilize the system and by combining it with the desired trajectory, the space manipulator could track the desired trajectory while suppressing system vibrations. In the latter, the trajectory planning and vibration suppression problems are transformed into an optimization problem and solved with particle swam optimization (PSO). In the context of pHRC, offline trajectory planning cannot be achieved because the manipulator is expected to follow human intentions in real time. In [11], a novel variable-speed control moment gyros (VSCMGs) is presented for vibration suppression. However, the proposed actuators may be difficult to implement because it requires major upgrades to the manipulator's mechanical system.

III. Experiment Setup

To investigate how compliance affects human performance during pHRC, the system that incorporates varying compliance levels and allows physical human-robot collaboration is set up as shown in Fig. 2 and Fig. 3. The system consists of a collaborative robot mounted on a rigid pedestal; an inertial measurement unit (IMU); an electromagnetic (EM) tracking system; a 6-axis force-torque (FT) sensor; soft foam sheets; an air bellow; a pneumatic regulator and a custom made handle that contains a safety trigger and a laser diode integrated inside.

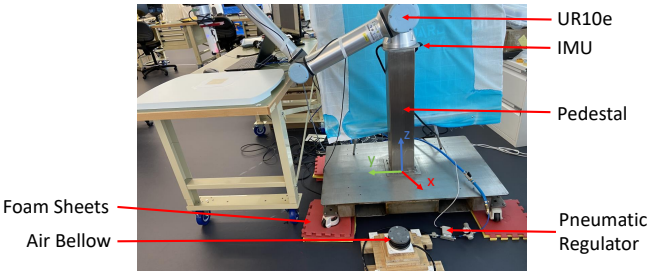

Fig. 2. System setup for the experiment

A. Task Design

The task design for the experiment is shown in Fig. 3. Inspired by and extending the widely adopted point-to-point task in human-robot co-operation and co-manipulation [14]–[16], a square trajectory is used for the experiment. The square reference trajectory with 100 mm side length is printed on an A4 sheet and affixed onto the tabletop. A handle with a laser pointer diode and an enabling safety switch is attached at the end-effector of the cobot to allow human-robot collaboration. The laser pointer projects a visible dot onto the paper to indicate its position. The task is to control the motions of the cobot through the handle such that the laser pointer completes 3 laps of the reference trajectory at a reasonable speed (about 7 seconds per loop) while maintaining high task accuracy.

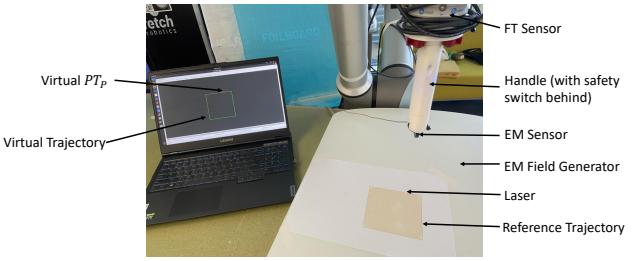

Fig. 3. The experiment task. The human grasps the handle and collaborates with the cobot to use the laser pointer to complete the reference trajectory.

B. Collaborative Robot

The collaborative robot used in the experiment is the 6-DOF (degree of freedom) Universal Robot UR10e mounted on a rigid pedestal. With consideration of the experimental task as introduced in the previous section, the cobot's motions are restricted to the x-y plane and it is controlled by an inertia-damping admittance control (AC) [17] at $500Hz$ using admittance control law (1).

$$M_d\ddot{x} + D_d\dot{x} = F \tag{1}$$

The controller takes the interaction force/torque $F \in \mathbb{R}^{6\times1}$ (measured from the F/T sensor) as input and computes the desired end-effector task space velocity $\dot{x} \in \mathbb{R}^{6\times1}$ according to (1). Then, $\dot{x}$ is converted from Cartesian to joint space velocity $\dot{q} \in \mathbb{R}^{6\times1}$ through inverse kinematics for the cobot to execute.

$M_d \in \mathbb{R}^{6\times6}$ and $D_d \in \mathbb{R}^{6\times6}$ in (1) are the positive-definite virtual inertia and damping matrices respectively. They can be tuned to create varying cobot admittance and therefore result in different human interaction experiences: in the case of low M_d and D_d values, high admittance is created and the cobot is easy to move. However, the system's stability and task accuracy can be compromised; When large M_d and D_d are implemented, the cobot has low admittance, it requires more physical effort to move but generally becomes more stable and easier for fine manipulations [18].

Due to the restricted motion of the end-effector, along the diagonals of M_d and D_d, only the values of the elements corresponding to the x-y planar motion are experimentally explored. Three levels of admittance values for x and y linear motions were chosen as shown in Table I, where m and d are the inertia and damping elements, respectively.

TABLE I

AC PARAMETERS USED IN THIS STUDY.

AC Parameters	Admittance Level	m ($k.g.$)	d (m/s)
1	High admittance	2	10
2	Medium admittance	4	25
3	Low admittance	6	40

C. Base Compliance Levels (BCL)

In order to produce different compliance levels in the system, soft foam sheets and an air bellow are placed underneath the cobot's pedestal to create base compliance. With the bellow deflated, the combined weight of the cobot and the pedestal compresses the foam sheets, leading to the system having a low level of compliance. By inflating the air bellow, it slightly lifts the pedestal from the foam so that a higher level of compliance is achieved. A pneumatic regulator is incorporated to control the volume of air used to inflate the air bellow, by controlling the input voltage of the pneumatic regulator, different base compliance levels (BCL) can be achieved.

For our system that is shown in Fig. 2, it is found that the air bellow predominantly generates *angular* compliance about the y-axis of the base. Compliance in other directions e.g. shear or translation, is very limited and can be neglected. The base compliance is modeled as a spring whose angular stiffness is estimated by

$$k = \tau/\alpha \tag{2}$$

where τ is the applied torque, and α is the angular displacement. Using the FT sensor to measure an applied torque, and an IMU attached rigidly to the pedestal, the angular stiffness of the base is estimated. As shown in Table II, four BCLs are used in the experiment: BCL 1 is with the air bellow completely deflated and the base is placed on the ground rigidly; BCLs 2, 3 and 4 have increasing levels of base compliance due to the bellow being inflated with increasing levels of air pressure.

TABLE II

BASE COMPLIANCE LEVELS USED IN THE EXPERIMENT.

Base Compliance Level (BCL)	y-axis Angular Stiffness (Nm/Degree)
1	1144.69
2	133.93
3	77.81
4	66.43

D. Electromagnetic (EM) Tracking System

When a cobot is mounted on a rigid base, the forward kinematics are typically all that is needed to calculate the pose of the cobot's end-effector since the base frame of the cobot is usually used as the world frame. However, with our cobot on a compliant base, the electromagnetic (EM) tracking system as shown in Fig. 3 needs to be used to provide the world frame for our experiment. A graphical illustration of the coordinate system of our experimental setup is demonstrated in Fig. 4. The coordinate frames for the cobot base, end-effector, EM sensor, EM field generator, laser and the sheet that contains the reference trajectory are denoted by $\{Base\}$, $\{EE\}$, $\{EM\}$, $\{F\}$, $\{L\}$ and $\{P\}$ respectively. Three transformations (marked in red) are also defined: the transformation from $\{L\}$ to $\{EM\}$ denoted as T_L^{EM} which is fixed; the transformation from $\{F\}$ to $\{P\}$ denoted as T_F^P which is also fixed; and the transformation from $\{EM\}$ to $\{F\}$ denoted as T_{EM}^F which is provided by the EM sensor. Using the kinematic calibration method presented in [19], the laser pointer's position in the x-y plane of $\{\mathrm{P}\}$, denote as PT_p can be computed. The accuracy of PT_p is checked for all the BCLs, the results in Table III show that the magnitude of PT_P error is acceptable and it is consistent across 4 BCLs.

TABLE III

RESULTS OF VIRTUAL PT_P UNDER DIFFERENT BCLS.

	PT_P (x, y)			
Ground Truth	BCL 1	BCL 2	BCL 3	BCL 4
(0, 0)	(-0.25, -0.05)	(-0.37, 0.43)	(-0.39, 0.5)	(-0.32, 0.55)
(0, 100)	(-0.14, 100.18)	(-0.21, 99.8)	(-0.33, 99.97)	(-0.48, 99.98)
(-100, 100)	(-100.36, 99.85)	(-100.55, 99.79)	(-100.37, 99.85)	(-100.32, 99.82)
(-100, 0)	(-100.48, -0.05)	(-100.06, 0.01)	(-100.15, -0.05)	(-100.24, 0.01)
Average Error	(0.31, 0.11)	(0.30, 0.21)	(0.31, 0.18)	(0.34, 0.19)

E. Experiment Procedure

Considering the aforementioned 3 AC Parameters and 4 BCLs, twelve distinctive combinations can be achieved. Participants are asked to complete the experiment with all 12 combinations following the experimental sequence generated by the balanced Latin Square [20]. Throughout the entire experiment, the combination of AC Parameters and BCL, as

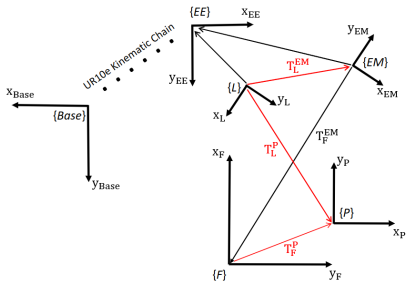

Fig. 4. Coordinate system for the experimental setup. The transformations T_L^{EM} and T_F^P are fixed and were estimated using the Matlab Optimization toolbox; T_F^{EM} is measured by the EM sensor; T_L^P is obtained by $T_F^P T_{EM}^F T_L^{EM}$.

well as the experimental sequence, are kept unbeknownst to participants.

First, participants are introduced to the experiment. The task design (Section III-A) are explained verbally, and a demonstration of the experiment is provided. Next, participants are given a few minutes to practice with the cobot. During the practice phase, BCL 1 and AC Parameters 2 are used. The task speed is monitored during practice and feedback is given to let participants know whether they need to move faster or slow down. The experiment commences when participants can achieve the expected speed consistently (about 7 seconds per loop). To keep participants engaged throughout the experiment, the total experiment time (including the verbal introduction and practice time) for each participant is limited to under 15 minutes. Previous trials found that participants began to lose focus when the duration of a pHRC experiment exceeded this length. After the experiment, the participants are reimbursed (a $10 gift card) for their time. The experiment was performed in the University of Technology Sydney (UTS) Robotics Institute (RI) laboratory under UTS Human Research Ethics Committee Approval ETH22-7370.

IV. Results

A total of 36 experimental subjects were recruited for the experiment. They are categorized into 2 cohorts according to their pHRC experience: *experienced* and *inexperienced*. For the experienced cohort, 12 people (11 males and 1 female) were recruited within the UTS RI laboratory. For the inexperienced cohort, 24 people (16 males and 8 females) were recruited through personal connections and incidental engagements at UTS. All the participants followed the experimental protocol strictly so that each combination of AC Parameters and BCL was repeated 36 times. In total, 432 sets of data which consist of the collaboration force, end-effector velocity and PT_p are collected on the Robot Operating System (ROS) platform.

In the analysis below, t_0 and t_f denote the experiment start time and finish time respectively; T is the number of sensor measurements, the subscripts $i \in \{1, \ldots, 12\}$ denotes different combinations of AC and BCL, and the superscript $n \in \{12, 24\}$ is the size of cohort.

A. Physical Effort

The physical effort is measured using the collaborative force in the x-y plane. For the i-th combination of AC and BCL, the average magnitude of the collaborative force F_m is computed by $F_m^i = \frac{1}{n}\sum_1^n(\frac{1}{T_n^i}\sum_{t_0}^{t_f}||F_n^i(t)||)$ where $||F_n^i(t)||$ is the magnitude of the collaborative force in the x-y plane, measured at timestep t with respect to $\{Base\}$. The results are presented in Fig. 5 for both cohorts.

First, it is observed that the average values and standard deviations of the inexperienced cohort are larger than those of the experienced cohort for all 12 combinations of AC and BCL. This reflects that the operator's experience has an effect on physical effort: less experienced human operators will exert a larger collaborative force during pHRC and the variation between subjects will be larger, too.

From the results, the effects of AC Parameters and BCL can be clearly perceived as well. For the former, the required collaboration force rises discernibly with the increases in the AC's virtual inertia and damping parameters for all the BCLs and across both cohorts. This result directly reflects the characteristics of AC as introduced previously: increased AC parameters will decrease the admittance of the cobot, and more physical effort is required to execute the task. On the other hand, when different BCLs are deployed under the same AC Parameters, the variation in the collaborative force is very narrow for all 3 AC Parameters among both cohorts. From these results, it can be viewed that the physical effort is mostly affected by the operator's experience and AC Parameters, not by the base compliance.

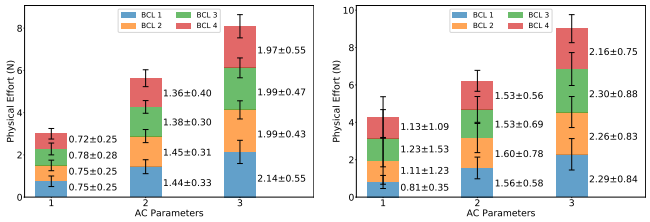

(a) Experienced Cohort (b) Inexperienced Cohort

Fig. 5. Magnitude of the mean collaborative force for (a) the experienced cohort and (b) the inexperienced cohort. The inexperienced cohort have exerted more collaborative force than the experienced cohort and their standard deviations are also larger, indicating the human experience has an impact on physical effort. When examining the unicolor bars across AC Parameters, a persistent rising trend can be observed for all 4 BCLs. On the other hand, for each set of AC Parameters, narrow and arbitrary variations can be noted when comparing the size of coloured bars. These results are indicating that physical effort is directly influenced by AC Parameters, and BCL has a very limited impact. Similar results are seen in both experienced and inexperienced cohorts.

B. Task Velocity

The average magnitude of task velocity V_m for the i-th combination of AC Parameters and BCL is computed by $V_m^i = \frac{1}{n}\sum_1^n(\frac{1}{T_n^i}\sum_{t_0}^{t_f}||V_n^i(t)||)$ where $||V_n^i(t)||$ is the magnitude of PT_P velocity in the x-y plane at timestep t. The results are shown in Fig. 6.

By comparing the task velocity values between the two cohorts, it is observed that the inexperienced cohort has

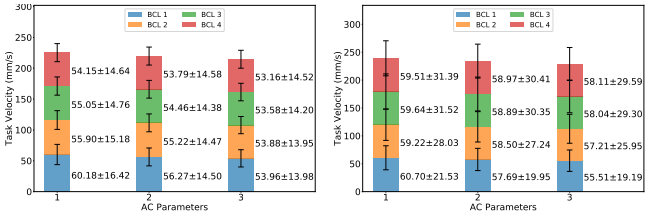

(a) Experienced Cohort (b) Inexperienced Cohort

Fig. 6. Magnitude of the mean task velocity for (a) the experienced cohort and (b) the inexperienced cohort. The inexperienced cohort achieved a higher task velocity than the experienced cohort for the AC and BCL combinations because a larger collaborative force was exerted by this cohort. When comparing the bars in the vertical direction (varying the BCL and constant AC Parameters), small and inconsistent variations in task velocity can be observed. With AC Parameters tuned larger while BCL being kept at the same level (unicolor bars on the horizontal direction), both cohorts' results show decreases in end-effector velocity. These results demonstrate that task velocity is only impacted by AC Parameters and not by base compliance level.

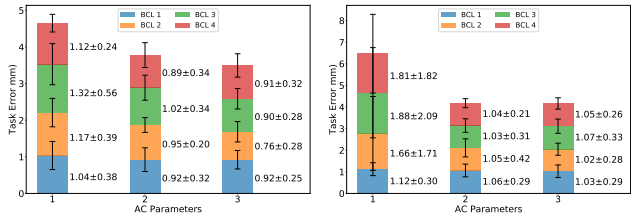

(a) Experienced Cohort (b) Inexperienced Cohort

Fig. 7. Average task error for (a) the experienced cohort and (b) the inexperienced cohort. Task error is impacted negatively by base compliance and positively by larger AC Parameters. By comparing the results on the same vertical axis, for AC Parameters 1, both cohorts' results show an increase in error as BCL increases from 1 to 4. When the larger AC Parameters 2 and 3 are utilized, both cohorts' performance in terms of task accuracy is not affected by BCL as significantly as before: task errors become consistent for different BCLs and reductions in error are achieved. The experience level also impacts the task error as it can be observed that the inexperienced cohort's task errors are consistently larger than those of the experienced cohort for all the experimental runs.

achieved a faster task velocity than the experienced cohort for all AC and BCL combinations. This result is closely related to the previous physical effort results because according to (1), higher velocity will be achieved with a higher collaborative force.

From both Fig. 6a and Fig. 6b, it can be observed that under the same AC Parameters, the variation of V_m with the increase in BCL is insignificant and arbitrary. This suggests the task velocity is not influenced by BCL. On the other hand, when studying the bars with the same color, a slight, consistent decreasing trend can be observed. This variation of V_m is attributed to the increasing AC parameters, which requires larger forces to move the end effector, leading to slower speeds despite the participants being asked to maintain a similar speed across trials. Similar to physical effort, the task velocity is also significantly influenced by AC Parameters and not by BCL.

C. Task Error

The average task error e for the i-th combination of AC and BCL is computed by $e^i = \frac{1}{n}\sum_1^n(\frac{1}{T_n^i}\sum_{t_0}^{t_f} d_n^i(t))$ where $d_n^i(t)$ is the Euclidean distance between PT_p and the virtual trajectory in the x-y plane at timestep t.

The results in Fig. 7 support that the task error is also influenced by the cohort's experience level. The inexperienced cohort generated larger errors than the experienced cohort for all combinations of AC and BCL. In addition to this, the following two observations can be made.

1) Base compliance has a negative impact on task accuracy: To examine the impact of base compliance on task accuracy, the errors produced under AC Parameters 1 are studied. Taking the BCL 1 error (when the pedestal is on most rigid) as the ground truth, the errors generated under BCLs 2, 3, and 4 are compared with it, and the ratios of change are computed. For the experienced cohort, the error for BCLs 2, 3 and 4 increase by *12.50%*, *26.92%* and *7.69%* respectively. For the inexperienced cohort, their respective increases in error are *63.96%*, *89.19%* and *88.46%*. From the figures and the numbers, it can be clearly seen that base compliance negatively impacts task accuracy when the AC Parameters are decreased.

2) Larger AC Parameters can reduce the task error initiated by base compliance: To examine how the AC Parameters reduces the task error, the above analysis can be carried out for AC Parameters 2 and 3. For AC Parameters 2 in Fig.7a, the experienced cohort's task error varies by *3.26%*, *10.87%* and *-3.26%* for BCLs 2, 3 and 4 respectively; with AC Parameters 3, the error varies by *-17.39%*, *-2.17%* and *-1.09%*. For the inexperienced cohort, their task error varied by *-3.57%*, *-6.25%* and *-8.04%* for AC Parameters 2 and *0.96%*, *1.92%* and *1.92%* for AC Parameters 3. The negative results imply reductions in error compared to the ground truth. Comparing these results with the AC Parameters 1 results above, the effectiveness of larger AC Parameters in reducing task error can be discovered. Moreover, considering the AC Parameters 1 results as the ground truth and comparing the unicolor bars located at AC Parameters 2 and 3 in Fig.7 to it, significant reductions in error can also be observed from both cohorts' results. For the experienced cohort, the error changes by *-11.54%* and *-11.54%* under BCL 1; *-18.80%* and *-35.04%* under BCL 2; *-22.73%* and *-31.82%* under BCL 3; *-20.54%* and *-18.75%* under BCL 4. For the inexperienced cohort, their average error changed by *0.90%* and *-6.31%* under BCL 1; *-40.66%* and *-42.31%* under BCL 2; *-50.00%* and *-49.52%* under BCL 3; *-47.45%* and *-45.92%* under BCL 4.

Through these results, it can be viewed that pHRC experience is helpful in reducing the task error and larger AC Parameters can effectively compensate for the base compliance to help human operators achieve higher task accuracy.

D. Analysis of Variance (ANOVA)

The quantitative results are evaluated with 3-way analysis of variance (ANOVA) to validate whether there are any statistically significant differences between the means of different

TABLE IV

RESULTS OF 3-WAY ANALYSIS OF VARIANCE (ANOVA) ON HOW THE INDEPENDENT FACTORS (PARTICIPANT'S EXPERIENCE, AC PARAMETERS AND BCL) AFFECT THE COLLABORATION FORCE, END-EFFECTOR VELOCITY AND TASK ERROR. FOR p-VALUE<0.05 (HIGHLIGHTED CELLS), IT INDICATES THE INDEPENDENT FACTOR HAS A SIGNIFICANT IMPACT ON THE DEPENDENT VARIABLES.

Independent Variable	Participant's Experience Level			AC Parameters			BCL		
Dependent Variable	Physical Effort	Task Velocity	Task Error	Physical Effort	Task Velocity	Task Error	Physical Effort	Task Velocity	Task Error
p-value	**0.0033**	0.0500	**0.0052**	**<0.001**	**<0.001**	**<0.001**	0.8689	0.8799	0.3004

groups of the independent factors. In this experiment, the independent factors are the *participants' experience level*, *AC Parameters* and *BCL*. ANOVA is conducted with the Matlab Statistics and Machine Learning Toolbox for the dependent variables of our experiment: *physical effort*, *task velocity* and *task error*. The ANOVA results are shown in Table IV. Generally, a p-value less than 0.05 indicates a strong effect due to the independent factor [21]. Using this standard significance level and from the highlighted cells, it can be viewed that the participant's experience level influences the physical effort and task error significantly as their respective p-values are *0.0033* and *0.0052*, and task velocity is not significantly impacted. However, it should be noted that the p-value for task velocity is lying on the cutoff of the standard significance level. The p-values of AC Parameters for all 3 dependent variables are small enough to conclude that AC Parameters have significant influences on physical effort, task velocity and task error. Lastly, the large p-values of BCL for all three dependent variables indicate that their mean responses for different BCLs are not significantly different, meaning that BCL does not influence the dependent variables critically. ANOVA provided the same results as obtained in the previous sections: physical effort and task error are significantly influenced by the participant's experience level and AC Parameters, and they are independent of BCL; task velocity is influenced predominantly by AC Parameters and potentially by the participant's experience level.

V. DISCUSSION

The experimental results show an interesting relationship between the level of base compliance and the admittance control parameters. Increasing the AC Parameters mitigates the poor task error introduced by increasing levels of base compliance. However, using large AC Parameters is not ideal because the level of admittance set by the AC Parameters was found to significantly affect physical effort and task velocity. This is not entirely surprising as the AC Parameters directly shape the interaction dynamics between the human and cobot as per (1). Larger admittance control parameters result in a higher physical workload for the human co-worker and reduces task time efficiency. Ideally, a control system for pHRC on a compliant base would be able to mitigate the negative affects of base compliance whilst achieving high task performance. If a mathematical model describing these effects can be derived, we envision that a pHRC control that accounts for the unwanted compliance while considering competing requirements may be developed. Regardless, understanding the implications of these effects is critical to enabling a high-performance pHRC on systems where base compliance is present.

A limitation of this study is the size of the experimental subjects. We recruited 36 participants for this study, such a size is sufficient to draw conclusions for the experiment. However, more experimental subjects will improve the robustness of the results. For example, in Table IV, the p-value which determines the influence of the participant's experience level on task velocity is 0.0500. This result is lying on the cut-off of the standard significance level, and more experimental data is required to validate the influence of the participant's experience level on task velocity.

Besides, only quantitative studies were carried out in our investigation. Qualitative results are also crucial in understanding pHRC. For example, in Section IV we have discovered the compromises between physical effort, task velocity and task accuracy. Qualitative analysis of the participant experience during the interaction was not carried out due to concerns about extended experiment durations leading to participants losing focus during the experiment. Future work should explore the qualitative impressions of users in response to differing levels of base compliance, assuming that an appropriate experimental protocol is used.

VI. CONCLUSIONS

In this paper, we presented an empirical study investigating the influences of base compliance on physical effort, task velocity and task error in a pHRC framework. A custom-made base whose compliance can be modulated was used. With 432 sets of data collected from 36 participants, we successfully validated that base compliance significantly and negatively influences task accuracy when low admittance control parameters are used. On the contrary, higher admittance control gains can stabilize the system effectively, but result in a higher demand for physical effort and reduce task efficiency. Moreover, human operator experience was found to have a positive impact on performance.

Although it is shown that base compliance is not the most influential factor in pHRC, it is still unclear as to the appropriate strategy that compensates for the errors initiated from the base compliance while providing a good balance between the required physical effort for collaboration and task speed. The outcomes of this paper motivate continued research in this area, such as the modeling of the compliant motion and the optimization control.

REFERENCES

[1] A. Hameed, A. Ordys, J. Możaryn, and A. Sibilska-Mroziewicz, "Control system design and methods for collaborative robots: Review," *Applied Sciences*, vol. 13, no. 1, 2023.

[2] M. G. Carmichael, S. Aldini, R. Khonasty, A. Tran, C. Reeks, D. Liu, K. J. Waldron, and G. Dissanayake, "The anbot: An intelligent robotic co-worker for industrial abrasive blasting," in *2019 IEEE/RSJ International Conference on Intelligent Robots and Systems (IROS)*, pp. 8026–8033, 2019.

[3] L. Peternel, N. Tsagarakis, D. Caldwell, and A. Ajoudani, "Adaptation of robot physical behaviour to human fatigue in human-robot co-manipulation," in *2016 IEEE-RAS 16th International Conference on Humanoid Robots (Humanoids)*, pp. 489–494, 2016.

[4] B. Whitsell and P. Artemiadis, "Physical human–robot interaction (phri) in 6 dof with asymmetric cooperation," *IEEE Access*, vol. 5, pp. 10834–10845, 2017.

[5] X. Fu, H. Ai, and L. Chen, "Integrated fixed time sliding mode control for motion and vibration of space robot with fully flexible base–link–joint," *Applied Sciences*, vol. 11, no. 24, p. 11685, 2021. Copyright - © 2021 by the authors. Licensee MDPI, Basel, Switzerland. This article is an open access article distributed under the terms and conditions of the Creative Commons Attribution (CC BY) license (https://creativecommons.org/licenses/by/4.0/). Notwithstanding the ProQuest Terms and Conditions, you may use this content in accordance with the terms of the License; Last updated - 2022-02-01.

[6] X. Yu, "Hybrid-trajectory based terminal sliding mode control of a flexible space manipulator with an elastic base," *Robotica*, vol. 38, pp. 550–563, 03 2020. Copyright - © Cambridge University Press 2019; Last updated - 2020-02-11.

[7] X. Huang, L. Chen, and D. Huang, "Pi sliding mode control and vibration suppression of a space robot with elastic base and two flexible arms," *IOP Conference Series.Materials Science and Engineering*, vol. 452, 12 2018. Copyright - © 2018. This work is published under http://creativecommons.org/licenses/by/3.0/ (the "License"). Notwithstanding the ProQuest Terms and Conditions, you may use this content in accordance with the terms of the License; Last updated - 2021-08-02.

[8] C. Feng, W. Chen, M. Shao, and S. Ni, "Trajectory tracking and adaptive fuzzy vibration control of multilink space manipulators with experimental validation," *Actuators*, vol. 12, no. 4, p. 138, 2023. Copyright - © 2023 by the authors. Licensee MDPI, Basel, Switzerland. This article is an open access article distributed under the terms and conditions of the Creative Commons Attribution (CC BY) license (https://creativecommons.org/licenses/by/4.0/). Notwithstanding the ProQuest Terms and Conditions, you may use this content in accordance with the terms of the License; Last updated - 2023-04-27.

[9] Z. Liu and J. Liu, *Dynamic Modeling and Vibration Control for a Nonlinear Three-Dimensional Flexible Manipulator*, pp. 137–171. 03 2020.

[10] J. Wang, F. Cao, and J. Liu, "Nonlinear partial differential equation modeling and adaptive fault-tolerant vibration control of flexible rotatable manipulator in three-dimensional space," *International Journal of Adaptive Control and Signal Processing*, vol. 35, no. 11, pp. 2138–2154, 2021.

[11] S. Jia and J. Shan, "Velocity-free trajectory tracking and active vibration control of flexible space manipulator," *IEEE Transactions on Aerospace and Electronic Systems*, vol. 58, no. 1, pp. 435–450, 2022.

[12] Y. Zhang, Y. Liu, Z. Xie, Y. Liu, C. Baoshi, and H. Liu, "Visual servo control of the macro/micro manipulator with base vibration suppression and backlash compensation," *Applied Sciences*, vol. 12, p. 8386, 08 2022.

[13] L. Cui, H. Wang, and W. Chen, "Trajectory planning of a spatial flexible manipulator for vibration suppression," *Robotics and Autonomous Systems*, vol. 123, p. 103316, 10 2019.

[14] A.-N. Sharkawy, P. Koustoumpardis, and N. Aspragathos, "A neural network-based approach for variable admittance control in human–robot cooperation: online adjustment of the virtual inertia," *Intelligent Service Robotics*, 10 2020.

[15] F. Dimeas and N. Aspragathos, "Reinforcement learning of variable admittance control for human-robot co-manipulation," in *2015 IEEE/RSJ International Conference on Intelligent Robots and Systems (IROS)*, pp. 1011–1016, 2015.

[16] B. Corteville, E. Aertbelien, H. Bruyninckx, J. De Schutter, and H. Van Brussel, "Human-inspired robot assistant for fast point-to-point movements," in *Proceedings 2007 IEEE International Conference on Robotics and Automation*, pp. 3639–3644, 2007.

[17] P. Song, Y. Yu, and X. Zhang, "A tutorial survey and comparison of impedance control on robotic manipulation," *Robotica*, vol. 37, no. 5, p. 801–836, 2019.

[18] A. Lecours, B. Mayer-St-Onge, and C. Gosselin, "Variable admittance control of a four-degree-of-freedom intelligent assist device," in *2012 IEEE International Conference on Robotics and Automation*, pp. 3903–3908, 2012.

[19] J.-S. Hu, J.-J. Wang, and Y.-J. Chang, "Kinematic calibration of manipulator using single laser pointer," in *2012 IEEE/RSJ International Conference on Intelligent Robots and Systems*, pp. 426–430, 2012.

[20] A. D. Keedwell and J. Dénes, "Chapter 1 - elementary properties," in *Latin Squares and their Applications (Second Edition)* (A. D. Keedwell and J. Dénes, eds.), pp. 1–36, Boston: North-Holland, second edition ed., 2015.

[21] F. Ferraguti, C. T. Landi, L. Sabattini, M. Bonfè, C. Fantuzzi, and C. Secchi, "A variable admittance control strategy for stable physical human–robot interaction," *The International Journal of Robotics Research*, vol. 38, no. 6, pp. 747–765, 2019.